Non-linear MHD simulations of ELMs

G.T.A. Huysmans, R. Abgrall[2], M. Becoulet, R. Huart[2], B. Nkonga[2], S. Pamela,
E. van der Plas, P. Ramet[3]

CEA, IRFM, F-13108 Saint-Paul-lez-Durance, France
[2]INRIA, Institut de Mathématiques, [3]LABRI, Université Bordeaux I, Bordeaux, France

Introduction

In recent years some progress has been made in the numerical simulation of Edge Localised Modes (ELMs) by means of non-linear MHD simulations of medium-n ballooning modes [1-5]. The MHD simulations are essential to improve our understanding of the physics of the ELMs (the onset, the amplitude of the crash, etc.) in view of the extrapolation to ITER and the control of ELMs. However, the simulation of a full ELM cycle remains an open problem.
In this paper we describe the recent developments of the non-linear MHD code JOREK and the application to the non-linear simulations of ELMs.

Numerical methods

The first ballooning mode simulations with the non-linear MHD code JOREK [4] used a very limited number of toroidal harmonics. In order to improve the resolution, the JOREK code has been undergone a significant development. The (R, Z) dependence of the MHD variables and the (R, Z) space coordinates are now discretised using the newly developed isoparametric bi-cubic Bezier finite elements [6]. The toroidal direction is discretised with Fourier harmonics. The definition of the new elements is based on so-called Bezier patches which are commonly used in computer aided design (CAD) applications. These Bezier finite elements are a generalisation of the well known cubic Hermite finite elements, as used for example in the HELENA equilibrium code. The generalisation allows the local refinement of each element, an essential step towards adaptive mesh refinement. With the isoparametric formulation, i.e. discretisation of (R, Z) using the same Bezier elements, the finite elements can be accurately aligned with the equilibrium flux surfaces on the closed and open field lines. The cubic elements combined with the alignment to the flux surfaces yield an accurate treatment of the large anisotropy in the temperature conductivity.
The time stepping scheme in the new version of the JOREK code remains fully implicit using the linearised Crank-Nicholson scheme on all the equations in one single step. In addition to the direct parallel sparse matrix solver (Pastix [8]), an iterative solver (GMRES) has been implemented using the sub-matrices of each toroidal harmonic as an efficient pre-conditioner (similar to a block-Jacobi preconditioning on a reordered matrix). This improves the scalability of the parallelisation of the code and alleviates the memory requirements of the fully implicit solver.
With a fully implicit method, there is no a priori limit on the time step. The time can be chosen on the scale of the physics of interest. In slow growing tearing modes cases, time steps of several thousand Alfven times are quite feasible.
The new version of the JOREK code has been verified on tearing mode and internal kink mode test cases. High order convergence of the linear growth rates (λ) with the grid size(h), $error(\lambda) \sim h^5$ has been confirmed.
In parallel to the JOREK code development, the code Fluidbox, a more general purpose CFD code, is being extended to include the full MHD model. Fluidbox uses a different numerical method: triangular type meshes (2D and 3D) and a stabilised residual distribution method [7] that is able to handle strong gradients and ensures monotinicity.

Reduced MHD, parallel velocity, boundary conditions

The reduced MHD model as implemented in the JOREK code has been extended to include the parallel flow velocity. This is an essential ingredient to study the parallel losses at the divertor plates. In the reduced MHD model, the magnetic field perturbations are described by a poloidal flux function in addition to a toroidal equilibrium field. The velocity field is described by the parallel velocity and a potential for the poloidal component:

$$\vec{B} = (F_0/R)\vec{e}_\varphi + (1/R)\vec{\nabla}\psi(t)\times\vec{e}_\varphi \qquad \vec{v} = -R\vec{\nabla}u(t)\times\vec{e}_\varphi + v_\parallel(t)\vec{B} \tag{1}$$

The following equations for the density ρ, temperature T, velocity $(u, v_\parallel)$ and poloidal flux ψ are implemented:

$$\frac{\partial\rho}{\partial t} = -\nabla\cdot(\rho\vec{v}) + \nabla\cdot\left(D_\perp\nabla_\perp\rho + D_\parallel\nabla_\parallel\rho\right) + S \qquad \rho\frac{\partial T}{\partial t} = -\rho v\cdot\nabla T - (\gamma-1)\rho T\nabla\cdot v + \nabla\cdot\left(\mathrm{K}_\perp\nabla_\perp T + \mathrm{K}_\parallel\nabla_\parallel T\right) + S_T$$

$$\vec{B}\cdot\left(\rho\frac{\partial\vec{v}}{\partial t} = -\rho\left(\vec{v}\cdot\vec{\nabla}\right)\vec{v} - \vec{\nabla}(\rho T) + \vec{J}\times\vec{B} + \mu\Delta\vec{v}\right) \qquad \vec{e}_\varphi\cdot\nabla\times\left(\rho\frac{\partial\vec{v}}{\partial t} = -\rho\left(\vec{v}\cdot\vec{\nabla}\right)\vec{v} - \vec{\nabla}(\rho T) + \vec{J}\times\vec{B} + \mu\Delta\vec{v}\right)$$

$$\frac{1}{R^2}\frac{\partial\psi}{\partial t} = +\eta\nabla\cdot\left(\frac{1}{R^2}\nabla_\perp\psi\right) - \vec{B}\cdot\nabla u \tag{2}$$

The boundary conditions at the main wall (typically aligned with a flux surface) are that all variables are constant in time. At the target where the field lines cross the boundary, the conditions on the density and temperature correspond to a free outflow. The velocity potential (i.e. electric potential) is left floating.

Application of the usual Bohm criterion on the parallel velocity, Mach one at the target, can lead to a large unphysical inflow of density and temperature at the target due to the poloidal component of the $E\times B$ flow due to an MHD instability.

To avoid this unphysical flow, a modified Bohm criterion is applied following Stangeby and Chankin [9]:

$$\vec{v}_\parallel\cdot\vec{n} + \vec{v}_E\cdot\vec{n} = \frac{\vec{v}_\parallel\cdot\vec{n}}{|v_\parallel|}c_s \tag{3}$$

where $\vec{n}$ is the normal at the target, c_s the local sound speed, $v_E = -R\nabla u\times e_\varphi$ the $E\times B$ flow. This condition ensures a positive outflow at the target at an 'equivalent' Mach one.

Non-linear MHD ELM simulations

The non-linear MHD simulation of an ELM evolves an x-point plasma with a typical H-mode edge pedestal where the pressure gradient exceeds the stability limit of medium-n ballooning modes. The initial 2D static equilibrium is evolved in time using only the axi-symmetric ($n=0$) harmonic. This leads to a quasi-steady but non-stationary equilibrium characterised by two flow components (see Fig. 1). The outflow boundary conditions on the parallel flow cause a large parallel flow close to the target. In addition, there is a localised poloidal flow (here with a poloidal m=1 structure) localised just inside the separatrix in the edge pedestal. The poloidal equilibrium flow is driven by the edge pressure gradient in combination with the resistivity and heat/particle diffusion (Pfirsch-Schluter flow).

Starting from this equilibrium, the $n=0$ to $n=18$ toroidal harmonics are evolved (with a periodicity of 3) with the parameters $\eta(0) = 2\times10^{-6}, D_\perp = \mathrm{K}_\perp = 10^{-5}$, $\mathrm{K}_\parallel = 10, \nu_\perp = 4\times10^{-6}$, $\nu_\parallel = 10^{-4}$. The time evolution of the magnetic energy is shown in Fig.2. The first 10^3 Alfven times show a phase exponential growth of the $n=6-15$ ballooning modes with a dominant $n=9$ mode. When the amplitude of the ballooning mode flow become of the order of the equilibrium flow, non-linear coupling causes a fast growth of all the toroidal harmonics. However, the linearly fastest growing mode remains dominant. The poloidal $E\times B$ flow pattern of the ballooning mode drives the outflow of the density into density filaments outside the separatrix. In agreement with previous results [4], the ballooning mode(s) induce a large

$n=0$ poloidal flow just inside the separatrix driven by the Maxwell stress. The density filaments are sheared off from the main plasma by this $n=0$ flow. The temperature perturbations are much smaller due to the large parallel conductivity. This is illustrated in figure 3 which shows the density, temperature and poloidal velocity potential in a poloidal plane at $t=2150\tau_A$. The coupling of several toroidal harmonics leads to a more localised mode structure in the toroidal and poloidal directions. After the initial bursts with a dominant $n=9$, the perturbation evolves towards the lower *n* mode numbers. During this phase the density filaments in the 'vacuum' are slowly (with the parallel velocity) moving towards the divertor.

The density profile in the mid plane (see Fig. 4) shows an outward moving density filament, similar to the fast density measurements during ELMs in MAST and JET. The local minimum in the density comes from a lower density inflow from a neighbouring poloidal region. The pressure profile in the pedestal before and at the end of the ELM (see Fig. 4) shows the reduction in the edge pressure gradient due to the ballooning mode.

With the implementation of the (simplified) divertor boundary conditions it becomes possible to evaluate the influence of the ELM (i.e. ballooning mode) on the profiles at the target. Figure 5 shows the temperature, density and parallel heat flux at the outer target. The temperature shows a fine structure on top of the usual radial decaying profile. The fine structure is due to the temperature perturbation, caused by the ballooning mode, extending beyond the separatrix. These temperature perturbations around the mid-plane are directly connected through the magnetic field lines to the divertor. The magnetic field maps these structures into a thin elongated form in the divertor (see Fig. 4). In the toroidal direction, this causes a spiral pattern at the target. The radial width at the target is about 1 cm. The simulation results are very similar to the infrared camera observations in AUG [10] of fine structure at the target. However, from the simulations it is clear that the fine structure is not necessarily evidence for filamentation of the temperature. The ballooning structure of the temperature perturbation beyond the separatrix is sufficient to create the fine structure at the target. The density perturbations (due to the absence of a large parallel transport) extend further into the SOL, leading to a strong broadening of the density profile at the target. These density perturbations causing the broadening arrive with the parallel velocity on a much slower timescale compared to the temperature perturbations.

Conclusion

The new developments of the JOREK code allow 3D non-linear MHD simulations of ELMs. The ELM simulations shows features similar to experimental observations such as the formation of (density) filaments and fine structure on the divertor target temperature profile.

This work, supported by the European Communities under the contract of Association between EURATOM and CEA, was carried out as part of the project ANR-CIS.2006.00 and has benefited from financial support from the French 'Agence National de la Recherche'. The views and opinions expressed herein do not necessarily reflect those of the European Commission.

References

[1] A.Y. Pankin et al., *Plasma Phys. Control. Fusion* **49** No 7 (July 2007) S63-S75
[2] H.R. Strauss et al., *Proc. 21st Int. Conf. on Fusion Energy 2006,(Chengdu, 2006)*
[3] N. Mizuguchi et al., *Nucl. Fusion* **47** No 7 (July 2007) 579-585
[4] G.T.A. Huysmans and O. Czarny, *Nucl. Fusion* **47** No 7 (July 2007) 659-666
[5] A.Y. Aydemir et al., *Physics of Plasmas*, **14**, 056118, 2007
[6] O. Czarny and G.T.A. Huysmans, accepted for publication in *J. Comp. Physics* (2008)
[7] R. Abgrall, *J. Comput. Phys.*, 2006, Vol. 214, No. 2, p.773-808.
[8] P. Hénon, P. Ramet and J. Roman, *Parallel Computing*, 2001, Vol. 28, No.2, p.301-321
[9] P.C. Stangeby and A.V. Chankin, *Physics of Plasmas*, 1995, 2, p.707
[10] T. Eich et al., *Plasma Phys. Control. Fusion* **47** (2005) 815–842

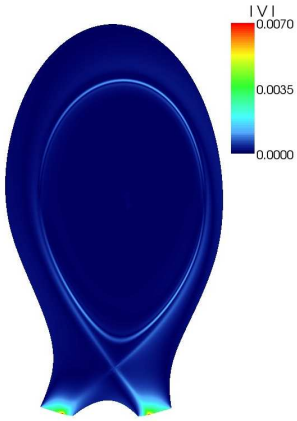

Fig. 1 *The total (poloidal and parallel) flow in the 'H-mode' equilibrium with edge pressure pedestal.*

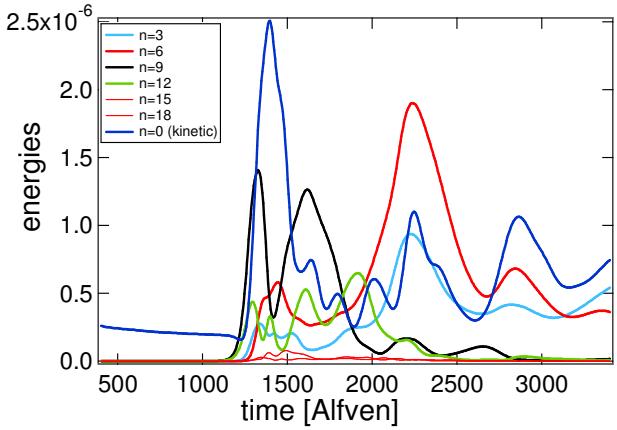

Fig. 2 *Evolution of the magnetic energy of the toroidal harmonics of the ballooning mode(s). Also shown is the n=0 kinetic energy.*

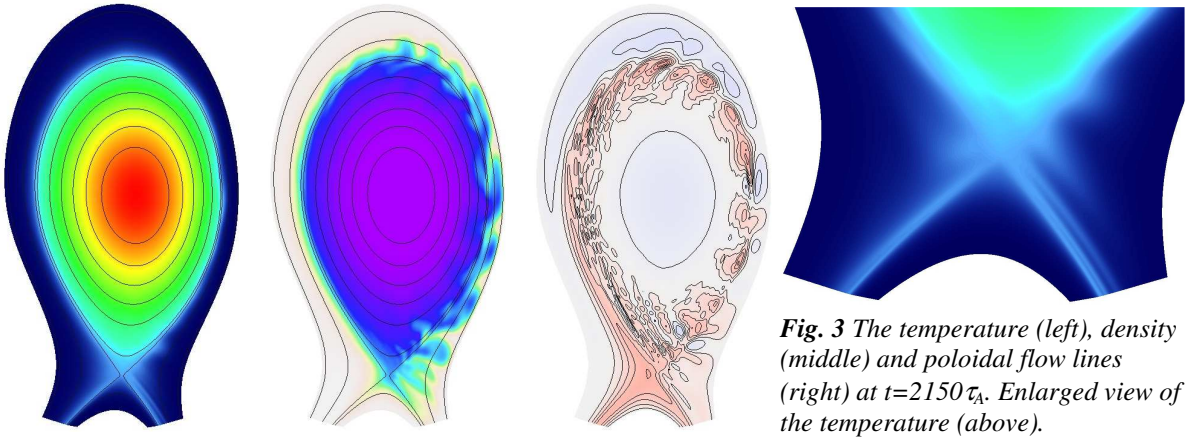

Fig. 3 *The temperature (left), density (middle) and poloidal flow lines (right) at t=2150 τ_A. Enlarged view of the temperature (above).*

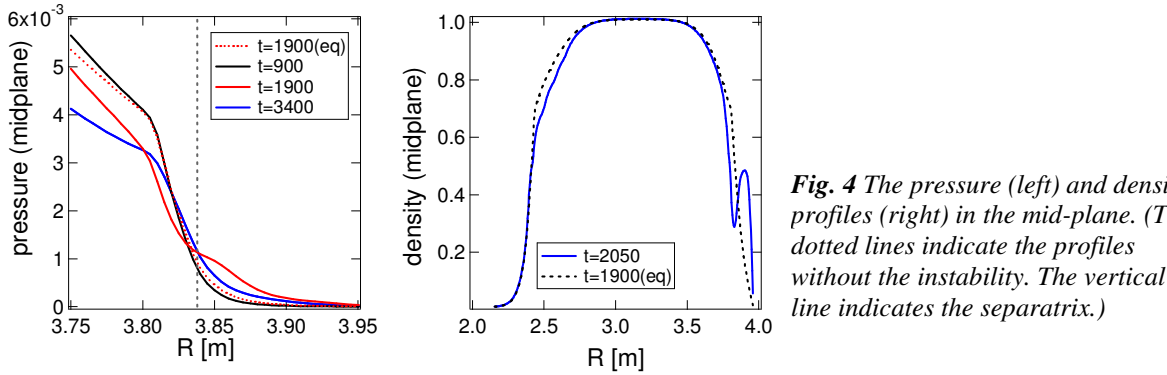

Fig. 4 *The pressure (left) and density profiles (right) in the mid-plane. (The dotted lines indicate the profiles without the instability. The vertical line indicates the separatrix.)*

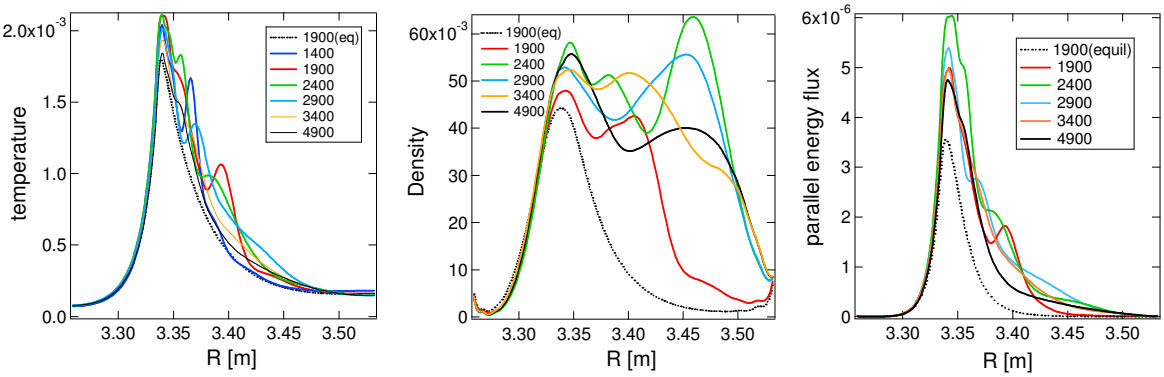

Fig. 5 *The temperature, density and parallel energy flux profiles at the outer target at several time slices during the ELM simulation. (The dotted lines show the profiles without the instability.)*